Continuum model of surface roughening and epitaxial breakdown during low-temperature Ge(001) molecular beam epitaxy

K. A. Bratland,[1] T. Spila,[1] D. G. Cahill,[1] J. E. Greene,[1] and P. Desjardins[2,a)]
[1]*Frederick Seitz Materials Research Laboratory and the Materials Science and Engineering Department, University of Illinois, 104 South Goodwin Avenue, Urbana, Illinois 61801, USA*
[2]*Regroupement québécois sur les matériaux de pointe and Département de génie physique, École Polytechnique de Montréal, P.O. Box 6079, Station Centre-Ville, Montréal, Québec H3C 3A7, Canada*

(Received 15 December 2010; accepted 15 January 2011; published online 21 March 2011)

Numerical simulations based on a discrete model describing step edge motion are used to compute the surface morphological evolution of Ge(001) layers deposited by low-temperature ($T_s = 45$–230 °C) molecular beam epitaxy and to probe the relationship between surface roughening and the onset of epitaxial breakdown—the abrupt growth mode transition from epitaxial to amorphous—at temperature-dependent critical film thicknesses $h_1(T_s)$. Computed surface widths w and in-plane coherence lengths d as a function of layer thickness h exhibit good agreement with experimental values. Inspired by experimental results indicating that epitaxial breakdown is initiated at facetted interisland trenches as the surface roughness reaches a T_s-independent overall aspect ratio, we show that simulated data for $w/d = 0.03$ correspond to thicknesses $h_1 \propto \exp(-E_1/kT_s)$ with $E_1 = 0.63$ eV, a value equal to the Ge adatom diffusion activation energy on Ge(001). Simulated h_1 values agree well with experimental data. Above a critical growth temperature of 170 °C, computed w/d values saturate at large film thicknesses, never reaching the critical aspect ratio $w/d = 0.03$. Thus, the model also predicts that epitaxial breakdown does not occur for $T_s > 170$ °C as observed experimentally.
 [doi:10.1063/1.3556745]

I. INTRODUCTION

The growth front during low-temperature (LT) homoepitaxy of group-IV (Refs. 1–10) and III-V (Refs. 3 and 11) semiconductors exhibits an abrupt structural breakdown once a critical film thickness is reached. This also occurs during LT heteroepitaxial growth, but the kinetics can be strongly mediated by strain.[12–17]

We have shown previously, using LT molecular beam epitaxy (MBE) of Ge/Ge(001), that epitaxial breakdown is a growth mode transition driven by kinetic surface roughening.[10] Ge(001) homoepitaxy in the low adatom mobility two-dimensional multilayer growth mode leads to the formation of a periodic array of self-organized mound structures preferentially bounded along ⟨100⟩ directions.[6,9,10] Surface widths w and in-plane coherence lengths d increase monotonically with film thickness h. Ge(001) layers grown at temperatures T_s greater than a critical value T_c remain fully epitaxial, while deposition at $T_s < T_c$ leads to a locally abrupt transition from epitaxial to amorphous growth.[10] This transition is initiated at a temperature-dependent critical thickness $h_1(T_s)$ as the surface roughness reaches a critical aspect ratio w/d which is independent of T_s.[10] $h_1(T_s)$ follows the relationship $h_1 \propto \exp(-E_1/kT_s)$, where $E_1 = 0.63$ eV.

An atomistic description of epitaxial breakdown during LT growth, based upon a combination of plan-view transmission electron microscopy (TEM), cross-sectional TEM (XTEM), and atomic force microscopy results, was proposed in Ref. 10 and is summarized here. During the early stages of deposition, the surface remains smooth, with a roughness comparable to that of the substrate. However, low adatom mobilities combined with an attachment asymmetry due to the presence of a positive Ehrlich barrier[18–22] at down-steps, and/or preferential attachment at up-steps, soon lead to a divergence in adatom flux and, hence, increased nucleation on terraces. As growth continues and the multilevel islands coalesce, trenches are formed which become deeper and wider, i.e., the amplitude of the roughness increases, as deposition proceeds. Incomplete filling of terraces results in the development of deep cusps bounded by {11l} facets, where $l = 7$, 5, 3, which eventually transform to low-energy {111} surfaces. Atomic shadowing in the cusps results in incomplete island coalescence and the subsequent formation of intercolumnar voids.

The transition from epitaxial to amorphous growth is initiated on {111} facetted cusps, where 111 stacking faults form due to double-positioning defects. The stacking faults quickly progress vertically and laterally along {111} facet planes. The initial transformation from crystalline to amorphous occurs in the cusps, with the regions between adjacent valleys still epitaxial. The growth mode transition is completed as 111 stacking faults at cusps on opposite corners or sides of individual islands intersect, resulting in a continuous epitaxial/amorphous interface which is globally rough but locally abrupt, as observed in XTEM images. In this description of LT epitaxial breakdown, the essential parameters, at a given T_s, are the adatom surface diffusion barrier E_m, the Ehrlich step-edge barrier E_b, and the vapor flux F.

Here, we use Villain's model of surface instabilities[23,24] to quantitatively describe the evolution of Ge(001) surface

a)Author to whom correspondence should be addressed. Electronic mail: patrick.desjardins@polymtl.ca.

roughness w as a function of film thickness h and growth temperature T_s in order to probe the relationship between surface roughening and epitaxial breakdown and test the above picture of surface morphological evolution. Our simulation results accurately reproduce experimental observations.

II. MODEL

Surface roughening is modeled following the approach of Elkinani and Villain[23–26] who derived continuum equations for the motion of step edges. The model involves two characteristic length scales: the nucleation length l_c and the Ehrlich length l_E.[23,24] l_c is the terrace width required to nucleate a new island, whereas l_E is defined such that if the terrace width l is smaller than l_E, atoms landing on this terrace migrate to, and are incorporated at, an up-step; however, if $l \gg l_E$, approximately half of the atoms that land on the terrace will migrate to the up step and half to the down step.

A schematic illustration of a typical growing (1+1)-dimensional crystal is presented in Fig. 1. The local step velocity is expressed as

$$v_n = f(l_n) + f(l_{n+1}), \tag{1}$$

where l_n and l_{n+1} are the widths of the terraces above and below the step edge, respectively.[25] For vicinal terraces,

$$f(l_n) = \frac{bFl_n}{2}\left(1 - \frac{l_E}{l_n + l_E}\right) \tag{2}$$

and

$$f(l_{n+1}) = \frac{bFl_{n+1}}{2}\left(1 + \frac{l_E}{l_{n+1} + l_E}\right). \tag{3}$$

When a terrace adjacent to the step edge is an island peak or valley, i.e. the local top (maximum) or bottom (minimum) terrace, the functions $f(l_{n,n+1})$ are defined as

$$f(l_{n,n+1}) = \frac{bFl_{n,n+1}}{2}. \tag{4}$$

New islands are created on terraces of width $l_{n,n+1}$ with a probability $P_{\text{nucl}}(l_{n,n+1})$ per unit time

$$P_{\text{nucl}}(l_{n,n+1}) = \frac{F^2 l_{n,n+1}^4}{12D}\left(1 + \frac{6l_E}{l_{n,n+1}^4}\right). \tag{5}$$

P_{nucl} becomes unity when $l_{n,n+1}$ becomes of order l_c. Adjacent step edges are limited to approaching within $b/2$ of each other [2.0 Å for the Ge(001) surface] although, in reality, the actual value chosen for the minimum step edge separation is irrelevant since l_c and l_E can be rescaled to modify the step spacing.

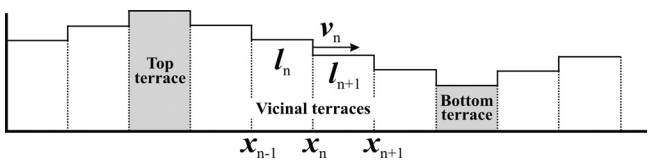

FIG. 1. Schematic surface profile during crystal growth.

Simulation input parameters include l_E, l_c, and the number of monolayers deposited. The output is an array showing the position and height of individual step edges for each simulated film thickness. Surface roughness as a function of film thickness is quantified using the height-height correlation function $H(\rho) = \langle h_i h_j \rangle$ and the height-difference correlation function $G(\rho) = \langle |h_i - h_j|^2 \rangle$, where $h_{i,j}$ are the heights at positions i and j separated by a distance ρ and the brackets correspond to averages over the measured surface. The mean interisland separation d is extracted from the position of the first local maximum in $H(\rho)$. The correlation functions are related to the surface width w, which is equivalent to the root mean square roughness, through the relationship $2w^2 = G(\rho) + 2H(\rho)$.

We determine the numerical values for the nucleation and Ehrlich lengths l_c and l_E for homoepitaxial Ge(001) growth by LT-MBE as a function of T_s based upon analyses of published *in situ* scanning tunneling microscopy (STM) data obtained during the early stages of surface roughening, well before the onset of epitaxial breakdown.[6,9] The simulated samples were of length $100l_c^2/l_E$ in order to maintain an equal number of islands at each temperature. The starting surface consists of terraces of length $l_0 = 810$ Å, which is equivalent to the average terrace length on the $\pm 0.1°$ miscut Ge(001) substrates used in Refs. 6, 9, and 10.

Figure 2 is a plot of l_c and l_E values for LT-MBE Ge(001) as a function of T_s.[6,9,27] l_c and l_E were extracted from STM data at $T_s = 60$, 100, 155, 175, and 230 °C using the relationships $l_c = n^{1/2}$ and $l_E = (dw/dh)^{1/2} l_c$ where n is the island density at a coverage of 0.3 ML and dw/dh is the roughening rate. As T_s is increased from 60 to 230 °C, l_c increases from 20 to 100 Å while corresponding l_E values remain nearly constant (approximately equal to the surface lattice spacing), decreasing slightly from 4.5 to 3.9 Å. The best fit to l_c vs T_s is shown by the dashed line which corresponds to

$$l_c = \left(\frac{20b^2 D}{F}\right)^{1/6}, \tag{6}$$

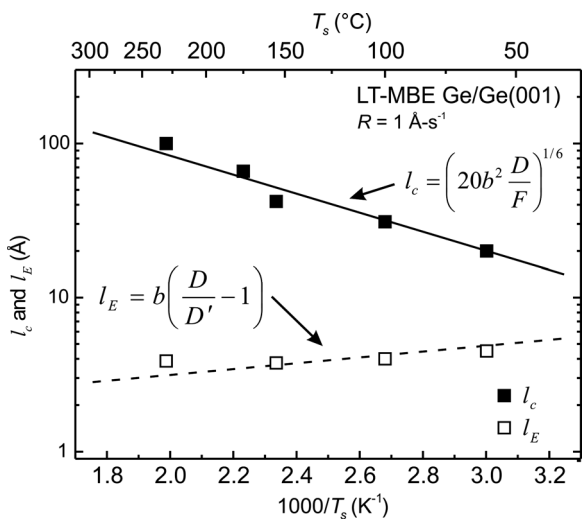

FIG. 2. Nucleation l_c and Ehrlich lengths l_E based upon STM data obtained during LT-MBE Ge(001) homoepitaxy over the temperature range $T_s = 60$–230 °C with $R = 1$ A s^{-1} (data from Refs. 9 and 27).

in which $b = 4.0$ Å is the separation between individual dimers along $\langle 110 \rangle$, F is the incident Ge flux in ML s^{-1}, $D = (b^2 v/4) \exp(-E_m/kT_s)$ is the surface diffusion constant, $E_m = 0.65$ eV (Ref. 9) is the activation energy for diffusion, and $v = 8.27 \times 10^{12}$ s^{-1} is the Ge Debye frequency.[28] Values for the dimer separation b and diffusion barrier E_m correspond to the direction parallel to the underlying dimer rows on the Ge(001)2×1 reconstructed surface. For simplicity, the incident flux is set at $F = 1$ ML s^{-1} yielding a deposition rate of $R = 1.4$ Å s^{-1}. A fit to l_E is obtained using the expression

$$l_E = b\left(\frac{D}{D'} - 1\right). \tag{7}$$

$D/D' = \exp(\Delta E_d/kT_s)$ with $\Delta E_d = 0.024$ eV the asymmetry in attachment activation energies at ascending and descending steps. $D'/b^2 = (v/4)\exp(-E_b/kT)$ is the adatom hopping rate over down steps.

III. RESULTS AND DISCUSSION

Typical simulated surface profiles obtained from layers deposited at $T_s = 155$ °C to thicknesses $h = 15$, 500, 2000, 4000, and 8100 Å are shown in Figs. 3(a)–3(e). The results show that the surface begins to roughen essentially immediately upon initiation of film growth. For small h values (≤ 500 Å at 155 °C), a high density of compact islands is obtained initially [e.g., Fig. 3(a) with $h = 15$ Å]. The mounds broaden, become better defined, and are separated by deep trenches as h is increased to 500 and 2000 Å [see Figs. 3(b) and 3(c)]. Continued island coalescence with increasing h results in a persistent increase in the mean interisland separation and a corresponding decrease in the island density. While $w(h)$ and $d(h)$ initially increase rapidly, they begin to saturate at $h > 2000$ Å [compare, for example, Fig. 3(d), $h = 4000$ Å with Fig. 3(e), $h = 8000$ Å]. Simulation results in Fig. 3 correlate well with experimental observations of Ge(001) surface roughening at $T_s = 155$ °C shown in Fig. 4 of Ref. 10. The same general trends are observed at all T_s values, but roughening and island coarsening rates increase with increasing T_s.

Figure 4 contains plots of calculated w and d values, together with the aspect ratio w/d, as a function of h and T_s. For clarity, only a representative sample of all simulated values is provided in Fig. 4. With $T_s \leq 100$ °C and $h \leq 1600$ Å, w and d both increase monotonically with h. w increases from 1.4 Å at $h = 10$ Å to 2.5 Å at $h = 60$ Å with $T_s = 45$ °C and from 1.3 Å at $h = 17$ to 7 Å at $h = 1600$ Å for $T_s = 85$ °C as d increases from 50 to 70 Å and from 85 to 185 Å over the same film thickness and temperature ranges. w and d follow scaling relationships $w \propto h^{\beta}$ and $d \propto h^{n}$ with roughening and coarsening exponents in this growth temperature range of $\beta \cong 0.4$ and $n \cong 0.2$. Thus, the mound roughening rate is larger than the coarsening rate. This leads, as shown in Fig. 4(c), to a slow increase in the aspect ratio w/d from 0.028 at $h = 10$ Å to 0.036 at $h = 60$ Å for $T_s = 45$ °C and

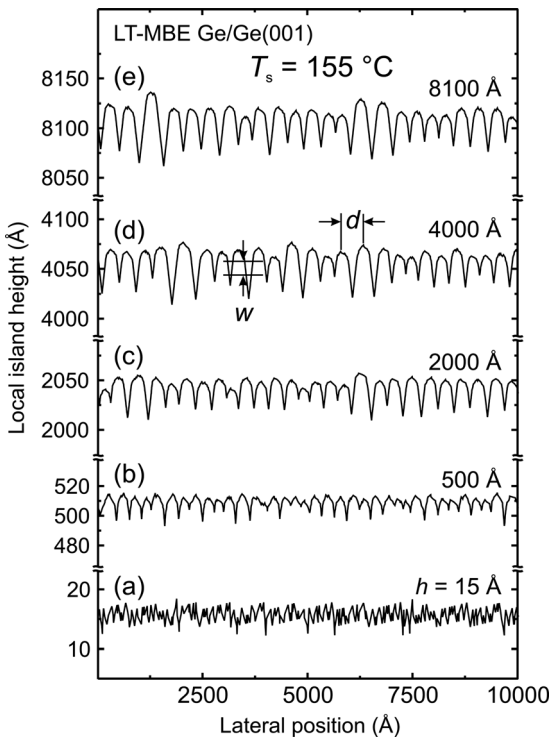

FIG. 3. Calculated surface height profiles for LT-MBE Ge/Ge(001) layers grown at $T_s = 155$ °C to thicknesses h of (a) 15, (b) 500, (c) 2000, (d) 4000, and (e) 8100 Å.

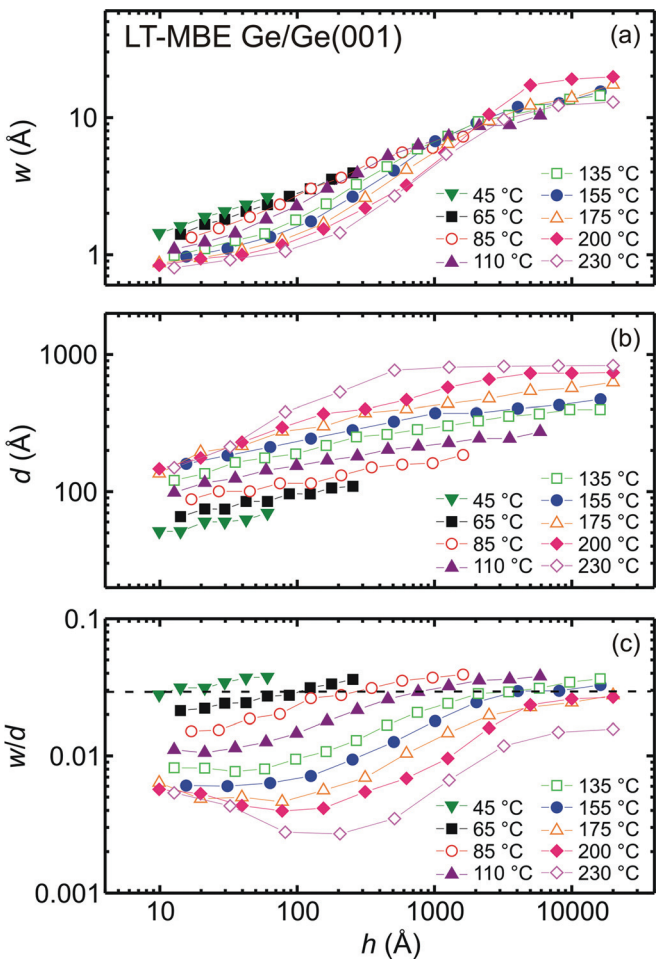

FIG. 4. (Color online) Calculated (a) surface widths w, (b) in-plane coherence lengths d, and (c) aspect ratios w/d as a function of film thickness h during Ge/Ge(001) LT-MBE at temperatures $T_s = 45$–230 °C.

from 0.015 at $h = 17$ Å to 0.038 at $h = 1600$ Å with $T_s = 85$ °C. The STM results of Van Nostrand and co-workers[6,9] for LT-MBE Ge(001) show that, with $T_s = 60$–100 °C, the experimentally determined roughening and coarsening exponents remain approximately constant at $\beta \cong 0.45$ and $n \cong 0.20$, respectively, in agreement with our simulated values over the same temperature ranges.

At higher growth temperatures ($T_s = 110$–230 °C), the simulated surfaces are initially flat with w of the order of 0.8–1.0 Å for the first few ML; then w increases linearly with h at a T_s-dependent rate. For layer thicknesses exceeding 3000 Å, w begins to saturate at h values of 10–20 Å with the saturation value being a function of temperature. $d(h)$ increases continuously with h, but otherwise follows the general behavior observed for $w(h)$. The saturation value of d increases with T_s from 400 Å at $T_s = 135$ °C to 850 Å at 230 °C, while the film thickness at which saturation begins to occur decreases from approximately 1 μm at $T_s = 135$ °C to 500 Å at 230 °C. The simulated roughening and coarsening exponents, as measured over the linear portion of the curves, increase from $\beta \cong 0.5$ and $n \cong 0.2$ at $T_s = 110$ °C to 0.7 and 0.3 at 230 °C. Experimentally, β and n increase continuously from 0.45 and 0.20, respectively, at $T_s = 100$ °C to 0.70 and 0.35 at $T_s = 230$ °C.[6,9,10]

A comparison of experimental and simulation results reveals that they exhibit good quantitative agreement. Figure 4(c) shows that over the temperature range 110–230 °C, the aspect ratio w/d is 0.006–0.010 initially and then begins to decrease as the island coarsening rate exceeds the roughening rate, allowing the surface to smoothen. With further increase in h, the calculated profiles now begin to roughen as the mounds grow faster vertically than laterally. Eventually, at large film thicknesses ($h > 3000$ Å), w/d saturates at values ranging from 0.040 at $T_s = 110$ °C to 0.015 at 230 °C.

We have previously demonstrated that epitaxial breakdown during Ge(001) LT-MBE is initiated at a film thickness $h = h_1(T_s)$ when the surface roughness reaches a critical T_s-independent aspect ratio.[10] These experimental results are captured in our simulation by defining h_1 as the film thickness at which the mound aspect ratio reaches a critical value $w/d = 0.03$. $h_1(w/d = 0.03)$ for each T_s in Fig. 4(c) is summarized in Fig. 5 as a phase map plotted as h_1 vs T_s (45–230 °C). The total set of simulation results is remarkably self-consistent over the entire temperature range and agree extremely well with h_1 values determined experimentally by both XTEM and reflection high-energy electron diffraction (experimental results also plotted in Fig. 5). h_1 increases exponentially with T_s and is well fit by the expression $h_1 \propto \exp(-E_1/kT_s)$ with $E_1 = 0.63 \pm 0.05$ eV.[4,10] The energy E_1 is equal to the measured activation barrier for Ge adatom diffusion on Ge(001).[9]

Since the thickness at which epitaxial breakdown is initiated can be modeled by defining $h_1(T_s)$ as the point at which the surface roughness reaches a critical aspect ratio, irrespective of T_s, there must be a direct relationship between the critical layer thicknesses plotted in Fig. 5 and adatom surface diffusivity. We have previously shown[10] that epitaxial breakdown is initiated when $x > L$, where x and L are the island peak-to-valley distance and adatom mean diffusion length, respectively. In this limit, adatoms can no longer fill the trenches during deposition. Epitaxial breakdown is initiated at $h \geq h_1$ as limited adatom mobilities lead to a reduction in the deposition rate at interisland trenches.

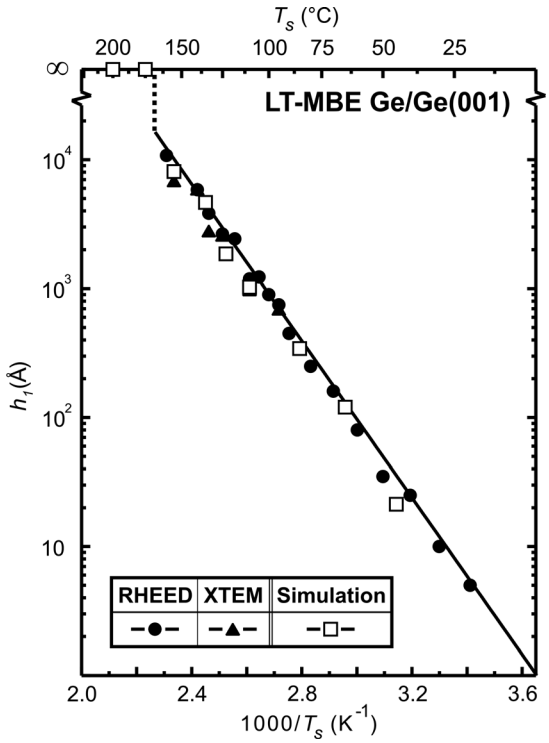

FIG. 5. Growth phase map obtained from simulations and LT-MBE experiments at $T_s = 45$–230 °C. The calculated data points correspond to the thicknesses h_1 at which the aspect ratio reaches a critical value $w/d = 0.03$. Experimental data is from Refs. 4 and 10.

Figure 4(c) shows that for $T_s > 170$ °C, the critical aspect ratio $w/d = 0.03$ is never reached. This indicates that infinitely thick epitaxial Ge(001) layers can be grown, in agreement with experimental results.[10] Thus, growth at $T_s > 170$ °C leads to the formation of mounds with slopes which, while still dependent on T_s, are no longer a function of h at large film thicknesses and, most importantly, w/d remains below 0.03.

In our simulation results, the values of the nucleation and Ehrlich lengths l_c and l_E, have been shown to play a crucial role in determining the average surface roughening rate and, hence, the epitaxial thickness. l_c and l_E are related to E_m and E_b, respectively, through Eqs. 6 and 7. Since $l_c \propto \exp(-E_m/kT_s)$ [see Eq. (6)], either a higher growth temperature T_s or a lower diffusion activation energy E_m (via, for example, surfactant effects as noted below) will produce a corresponding increase in l_c. Stated differently, an increase in the adatom mobility produces a corresponding increase in the minimum terrace width necessary to nucleate a new island. The Ehrlich length l_E is defined as the terrace width below which all adatoms migrate to an up-step and is proportional to $\exp(\Delta E_d/kT_s)$ [Eq. (7)]. An increase in T_s or a reduction in the adatom attachment asymmetry activation energy ΔE_d, both of which result in enhanced down-step crossing probabilities, give rise to a decrease in l_E.

Thus, a decrease (increase) in l_c and/or an increase (decrease) in l_E lead to a corresponding increase (decrease)

in the average roughening rate since the critical aspect ratio w/d is attained at a smaller (larger) film thickness. This has been demonstrated experimentally during the LT growth of Sn-doped Ge(001) layers.[16,17] Dilute Sn concentrations, 1×10^{18} cm^{-3} to <2.0 at. % at $T_s=155$ °C, act as a surfactant leading to a reduction in the ratio of the activation energies E_b/E_m and, hence, an increase in l_c/l_E. The net result is surface smoothening and a corresponding increase in the epitaxial thickness $h_1(T_s)$. As the Sn concentration is raised above 2.0 at. %, strain-induced roughening overcomes surfactant surface smoothening effects.

IV. CONCLUSION

We quantitatively describe the surface morphological evolution of Ge(001) layers during LT-MBE homoepitaxial growth with a numerical simulation based upon continuum equations for the motion of step edges. Using measured and extrapolated nucleation length l_c and Ehrlich length l_E values, we calculate surface roughness profiles to obtain the surface width w and in-plane coherence length d as a function of film thickness h and deposition temperature T_s. Calculated $w(h,T_s)$ and $d(h,T_s)$ results exhibit quantitative agreement with experimental data. We show that by defining a critical T_s-independent aspect ratio, $w/d=0.03$, the exponential dependence of the epitaxial thickness h_1 on temperature follows the relationship $h_1 \propto \exp(-E_1/kT_s)$, with $E_1=0.63\pm0.05$ eV, also in good agreement with experiment. Above a critical temperature $T_s=170$ °C, w/d saturates at large h values without having reached the critical aspect ratio, indicating that epitaxial breakdown no longer occurs, as observed experimentally. These results show that E_1 and T_c depend directly on l_c and l_E, respectively, which are determined, in turn, by E_m and E_b. The latter surface activation barriers can be altered through the addition of dilute surfactants such as Sn during LT-MBE Ge(001) as was demonstrated experimentally in Refs. 16 and 17.

ACKNOWLEDGMENTS

The authors gratefully acknowledge the financial support of the U.S. Department of Energy (DOE) under Grants Nos. DEFG02-07ER46453 and DEFG02-07ER46471 during the course of this research. They also appreciate the use of the facilities of the Center for Microanalysis of Materials, which is partially supported by the DOE, at the University of Illinois. P.D. thanks the Canada Research Chair Program and the Natural Sciences and Engineering Research Council of Canada for financial support.

[1]H. Jorke, H.-J. Herzog, and H. Kibbel, Phys. Rev. B **40**, 2005 (1989);H. Jorke, H. Kibbel, F. Schaffler, and H.-J. Herzog, Thin Solid Films **183**, 309 (1989).
[2]D. J. Eaglesham, H.-J. Gossman, and M. Cerullo, Phys. Rev. Lett. **65**, 1227 (1990).
[3]D. J. Eaglesham, H.-J. Gossman, M. Cerullo, L. N. Pfeiffer, and K. C. West, J. Cryst. Growth **111**, 833 (1991).
[4]G. Xue, H. Z. Xiao, M.-A. Hasan, J. E. Greene, and H. K. Birnbaum, J. Appl. Phys. **74**, 2512 (1993).
[5]N.-E. Lee, G. A. Tomasch, and J. E. Greene, Appl. Phys. Lett. **65**, 3236 (1994).
[6]J. E. Van Nostrand, S. J. Chey, M.-A. Hasan, D. G. Cahill, and J. E. Greene, Phys. Rev. Lett. **74**, 1127 (1995).
[7]N.-E. Lee, D. Cahill, and J. E. Greene, Phys. Rev. B **53**, 7876 (1996).
[8]O. P. Karpenko, S. M. Yalisove, and D. J. Eaglesham, J. Appl. Phys. **82**, 1157 (1997).
[9]J. E. Van Nostrand, S. J. Chey, and D. G. Cahill, Phys. Rev. B **57**, 12 536 (1998).
[10]K. A. Bratland, Y. L. Foo, J. A. N. T. Soares, T. Spila, P. Desjardins, and J. E. Greene, Phys. Rev. B **67**, 125322 (2003).
[11]D. J. Eaglesham, L. N. Pfeiffer, K. W. West, and D. R. Dykaar, Appl. Phys. Lett. **58**, 65 (1991).
[12]N.-E. Lee, G. Xue, and J. E. Greene, J. Appl. Phys. **80**, 2199 (1996).
[13]N.-E. Lee, M. Matsuoka, M. R. Sardela, F. Tian, and J. E. Greene, J. Appl. Phys. **80**, 812 (1996).
[14]O. Gürdal, P. Desjardins, J. R. A. Carlsson, N. Taylor, H. H. Radamson, J.-E. Sundgren, and J. E. Greene, J. Appl. Phys. **83**, 162 (1998).
[15]P. Desjardins, T. Spila, O. Gürdal, N. Taylor, and J. E. Greene, Phys. Rev. B **60**, 15 993 (1999).
[16]K. A. Bratland, Y. L. Foo, P. Desjardins, and J. E. Greene, Appl. Phys. Lett. **82**, 4247 (2003).
[17]K. A. Bratland, Y. L. Foo, T. Spila, H.-S. Seo, R. T. Haasch, P. Desjardins, and J. E. Greene, J. Appl. Phys. **97**, 44 904 (2005).
[18]G. Ehrlich and F. G. Hudda, J. Chem. Phys. **44**, 1039 (1966).
[19]S. C. Wang and G. Ehrlich, Phys. Rev. Lett. **70**, 41 (1993).
[20]S. C. Wang and G. Ehrlich, Phys. Rev. Lett. **71**, 4177 (1993).
[21]G. Ehrlich, Surf. Sci. **331/333**, 865 (1995).
[22]A. Gölzhäuser and G. Ehrlich, Phys. Rev. Lett. **77**, 1334 (1996).
[23]I. Elkinani and J. Villain, Solid State Commun. **87**, 105 (1993).
[24]P. Politi and J. Villain, Phys. Rev. B **54**, 5114 (1996).
[25]J. Villain, J. Phys. I **1**, 19 (1991).
[26]A. Pimpinelli and J. Villain, *Physics of Crystal Growth* (Cambridge University Press, Cambridge, 1998).
[27]J.E. Van Nostrand, Ph.D. thesis, University of Illinois at Urbana-Champaign, 1996.
[28]$\theta_D=375$ K for Ge (see Ref. 8) and $v=k\theta_D/h$ where k and h are Boltzmann's and Planck's constants, respectively.